

TABLE OF CONTENTS

	Page
Acknowledgements	iii
Abstract (English)	iv
Abstract (Thai)	vi
List of Tables	xii
List of Figures	xiv
Abbreviations and Symbols	xx
CHAPTER1 INTRODUCTION	1
1.1 Background	1
1.2 Titanium dioxide (TiO ₂)	3
1.3 Platinum (Pt)	5
1.4 Gold (Au)	7
1.5 Silver (Ag)	8
1.6 Flame spray pyrolysis (FSP)	10
1.7 Characterization techniques	12
1.7.1 X-ray diffraction method	12
1.7.2 Scanning Electron Microscopy	14
1.7.3 Transmission Electron Microscopy	17
1.7.4 The Brunauer-Emmett-Teller	20
1.8 Semiconductor gas sensors	22

1.8.1	Gas sensing mechanism	28
1.8.2	Catalytic additives on semiconducting oxide sensors	30
1.9	Literature reviews	34
1.10	Objectives of the study	42
1.11	Usefulness of the research (Theory and/or Applied)	43
1.12	Research plan, methodology and scope	43
CHAPTER 2	EXPERIMENTAL	44
2.1	Chemicals and equipment	44
2.2	Instruments	46
2.3	Sample preparations of unloaded TiO ₂ and metal-loaded TiO ₂ nanoparticles synthesized by FSP	47
2.4	Characterization of nanoparticles	53
2.5	Preparation and characterization of sensors	54
2.6	Gas sensing characterization	56
CHAPTER 3	RESULTS AND DISCUSSION	58
3.1	Characterization of unloaded TiO ₂ and metal-loaded TiO ₂ by FSP	58
3.1.1	X-ray diffraction analysis (XRD)	58
3.1.2	Scanning Electron Microscopy (SEM)	60
3.1.3	Energy Dispersive X-Ray Spectroscopy (EDS)	64
3.1.4	High resolution transmission electron microscopy (HRTEM)	66

3.1.5	BET analysis	68
3.1.6	Film thickness sensing layer	70
3.2	Gas sensor properties	71
3.2.1	Gas sensing of metal-loaded TiO ₂ nanoparticles synthesized by FSP towards hydrogen (H ₂) gas	72
3.2.2	Gas sensing of metal-loaded TiO ₂ nanoparticles synthesized by FSP towards ethanol gas	81
3.2.3	Gas sensing of metal-loaded TiO ₂ nanoparticles synthesized by FSP towards acetone gas	85
3.2.4	Gas sensing of metal-loaded TiO ₂ nanoparticles synthesized by FSP towards carbon monoxide gas	88
3.2.5	Gas sensing of metal-loaded TiO ₂ nanoparticles synthesized by FSP towards sulfur dioxide gas	91
3.2.6	Selective gas sensors based on flame-spray-made metal-loaded TiO ₂ nanoparticles	92
3.3	Summary of characteristics of unloaded TiO ₂ and metal-loaded TiO ₂ nanoparticles synthesized by FSP	95

CHAPTER 4 CONCLUSIONS 115

4.1	Nanoparticles synthesized by FSP	115
4.2	Comparison of characteristics of unloaded TiO ₂ and metal-loaded TiO ₂ nanoparticles synthesized by FSP	116
4.3	Gas sensing properties	117

4.4	Comparison of gas sensing response of unloaded TiO ₂ and metal-loaded TiO ₂ nanoparticles synthesized by FSP	118
4.5	Suggestions for the future work	120
REFERENCES		121
APPENDICES		140
Appendix A	INSTRUMENT	141
Appendix B	JCPDS INFORMATION	146
CURRICULUM VITAE		151

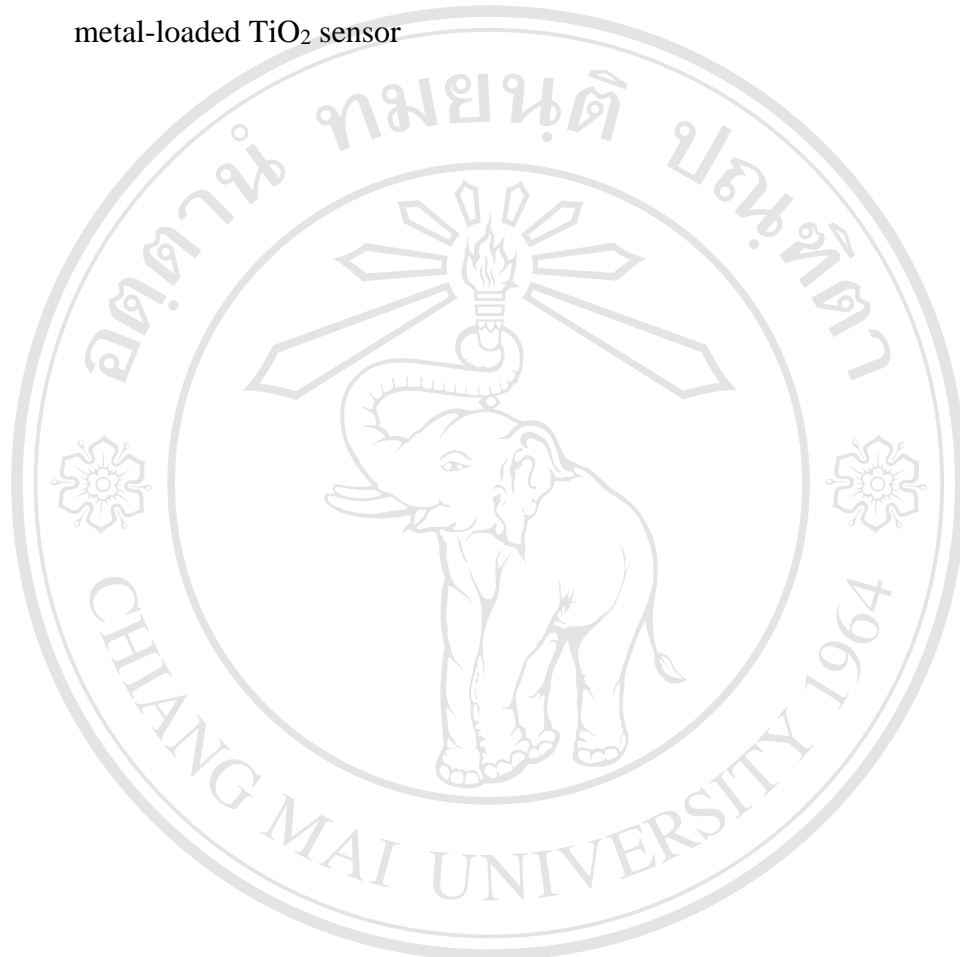


ลิขสิทธิ์มหาวิทยาลัยเชียงใหม่
Copyright© by Chiang Mai University
All rights reserved

LIST OF TABLES

Table	Page
1.1 Types and physical properties of titanium dioxide	4
1.2 Chemical and physical properties of Pt	6
1.3 Chemical and physical properties of Au	8
1.4 Chemical and physical properties of Ag	9
1.5 A summary on the gas sensing properties of differently prepared unloaded TiO ₂ and metal-loaded TiO ₂ towards reducing gas	39
2.1 Chemicals, Molecular formula, Molecular weight, Purity and Company	44
2.2 Instrument used in the experiments	46
2.3 Precursors calculation of the flame synthesis of 0–3.0 mol% Pt-loaded TiO ₂	48
2.4 Precursors calculation of the flame synthesis of 0–3.0 mol% Au-loaded TiO ₂	49
2.5 Precursors calculation of the flame synthesis of 0–3.0 mol% Ag-loaded TiO ₂	50
3.1 Summary of characteristics of unloaded TiO ₂ and Pt-loaded TiO ₂ nanoparticles synthesized by FSP	95
3.2 Summary of gas sensing performances of unloaded TiO ₂ and metal-loaded TiO ₂ sensor synthesized by FSP	96

4.1	Summary of characteristics of unloaded TiO ₂ and metal-loaded TiO ₂ nanoparticles	116
4.2	Summary of gas sensing performances of unloaded TiO ₂ and metal-loaded TiO ₂ sensor	119



ลิขสิทธิ์มหาวิทยาลัยเชียงใหม่
Copyright© by Chiang Mai University
All rights reserved

LIST OF FIGURES

Figure	Page
1.1 Schematic model of TiO_6 polyhedra for the TiO_2 phases rutile (a), anatase (b) and brookite (c) (Ti (white); O (red))	3
1.2 The periodic table of Pt element	6
1.3 The periodic table of Au element	7
1.4 The periodic table of Ag element	9
1.5 Formation of nanoparticles in flames. After evaporation and combustion of the precursors, particle formation starts by nucleation from the gas phase. These particles coagulate and, depending on the temperature, sinter into larger particles or agglomerate. In the case of supported noble metal catalysts, noble metal particle formation starts after support formation by homogeneous nucleation from the gas phase and/or heterogeneous nucleation on the support	11
1.6 Diffraction of X-rays by a crystal	13
1.7 A schematic drawing of a SEM microscope including the interactions between a bulk specimen and the incident e-beam	16
1.8 A schematic drawing of the interactions between an electron transparent specimen and the incident e-beam in a TEM	19

1.9	(a) Nanowire-pattern sensor device completed with circuitry elements; 25 the nanowire pattern is in the middle of the sample (high magnification in right bottom), whereas all around are the visible heater element and parallel electrode contacts for SnO ₂ nanowires. (b) Functional characterization of 80 nm wire-pattern sensor (solid line) and continuous film sensor (dotted line)	
1.10	The response and recovery time of n-type semiconductor for reducing gas	27
1.11	Schematics indicating the mechanisms leading to metal oxide sensor response to oxidizing and reducing gases	28
1.12	Catalytic additives on semiconducting oxide sensors. Top: Electrical sensitization-oxidation state of metallic clusters depend on ambient gases. Bottom: Chemical sensitization-metallic clusters promote the activation of gaseous specie	32
1.13	(a) Schematic depiction of the major process taking place at a metal oxide nanowire/nanobelt surface when exposed to O ₂ . (b) Band diagram of the pristine metal oxide nanostructure and in the vicinity (and beneath) a metal oxide nanoparticle. The radius of the depletion region is determined by the radius of the spillover zone	34
2.1	Schematic diagram of the experimental setup for the synthesis of metal-loaded TiO ₂ nanoparticles by FSP	51
2.2	Spray flame of (a) unloaded TiO ₂ , (b) Pt, (c) Au and (d) Ag-loaded TiO ₂ nanoparticles	52
2.3	The sensors preparation by spin coating technique	55
2.4	SEM images of (a) Al ₂ O ₃ substrates interdigitated with Au electrodes and (b) TiO ₂ films sensor on an Al ₂ O ₃ substrate interdigitate with Au electrodes	55

2.5	The experimental set up of sensing test	57
3.1	XRD patterns of flame-spray-made (5/5) unloaded TiO ₂ as-prepared, 0.25, 0.50, 0.75, 1.0, 2.0 and 3.0 mol% Pt (a), Au (b) and (c) Ag-loaded TiO ₂ samples	60
3.2	The morphology of highly crystalline flame-made (5/5) (a) unloaded TiO ₂ , (b) 0.25 mol% Au-loaded TiO ₂ , (c) 0.5 mol% Au-loaded TiO ₂ , (d) 0.75 mol% Au-loaded TiO ₂ , (e) 1.0 mol% Au-loaded TiO ₂ , (f) 2.0 mol% Au-loaded TiO ₂ and (g) 3.0 mol% Au-loaded TiO ₂ nanoparticles for SEM analysis	61
3.3	The morphology of highly crystalline flame-made (5/5) (a) 0.25 mol% Pt-loaded TiO ₂ , (b) 0.50 mol% Pt-loaded TiO ₂ , (c) 0.75 mol% Pt-loaded TiO ₂ , (d) 1.0 mol% Pt-loaded TiO ₂ , (e) 2.0 mol% Pt-loaded TiO ₂ and (f) 3.0 mol% Pt-loaded TiO ₂ nanoparticles for SEM analysis	62
3.4	The morphology of highly crystalline flame-made (5/5) (a) 0.25 mol% Ag-loaded TiO ₂ , (b) 0.50 mol% Ag-loaded TiO ₂ , (c) 0.75 mol% Ag-loaded TiO ₂ , (d) 1.0 mol% Ag-loaded TiO ₂ , (e) 2.0 mol% Ag-loaded TiO ₂ and (f) 3.0 mol% Ag-loaded TiO ₂ nanoparticles for SEM analysis	63
3.5	The EDS spectra images of all elements in the (a) unloaded TiO ₂ , (b) 0.50 mol% Pt-loaded TiO ₂ , (c) 1.0 mol% Au-loaded TiO ₂ and (d) 1.0 mol% Ag-loaded TiO ₂ nanoparticles	65
3.6	HRTEM images of (a) unloaded TiO ₂ , (b) 1.0 mol% Pt-loaded TiO ₂ , (c) 1.0 mol% Au-loaded TiO ₂ , (d) 1.0 mol% Ag-loaded TiO ₂ and (e) lattice fringes image of TiO ₂ nanoparticles	67

- 3.7 The specific surface area (SSA_{BET}) and d_{BET} of (a) Pt, (b) Au and (c) Ag-loaded TiO_2 nanoparticles 69
- 3.8 Cross-section SEM micrograph of gas sensing film based on flame-made (a) unloaded TiO_2 , (b) 0.50 mol% Pt-loaded TiO_2 , (c) 1.0 mol% Au-loaded TiO_2 and (d) 1.0 mol% Ag-loaded TiO_2 nanoparticles. 71
- 3.9 The change in resistance of metal-loaded TiO_2 sensors, under exposure to H_2 pulses with varying concentrations from 0.015 to 1.0 vol% 400 °C 73
- 3.10 The sensor response (S) (left axis) and response time (T_{res}) (right axis) versus H_2 concentration ranging from 0.015–1.0 vol% of 0.25, 0.50, 0.75, 1.0, 2.0 and 3.0 mol% (a) Pt, (b) Au and (c) Ag-loaded TiO_2 sensor at 300 °C 75
- 3.11 Electrical resistance change induced at 300, 350, and 400 °C for the thick films of 2.0 mol% Pt-loaded TiO_2 76
- 3.12 Variation of (a) Pt, (b) Au and (c) Ag-loaded TiO_2 sensor response to 1.0 vol% of H_2 with different the operating temperatures ranging from 300–400 °C 77
- 3.13 Schematic gas sensing mechanisms of Pt-loaded TiO_2 nanoparticles with (a) optimal Pt concentration and (b) excessive Pt concentration at high operating temperature (350–400 °C).concentration (3.0 mol%) at low operating temperature (300 °C) and (c) with optimal Pt 79
- 3.14 The change in resistance of metal-loaded TiO_2 sensors, under exposure to CH_3CH_2OH pulses with varying concentrations from 0.0050 to 0.10 vol% 350 °C 82

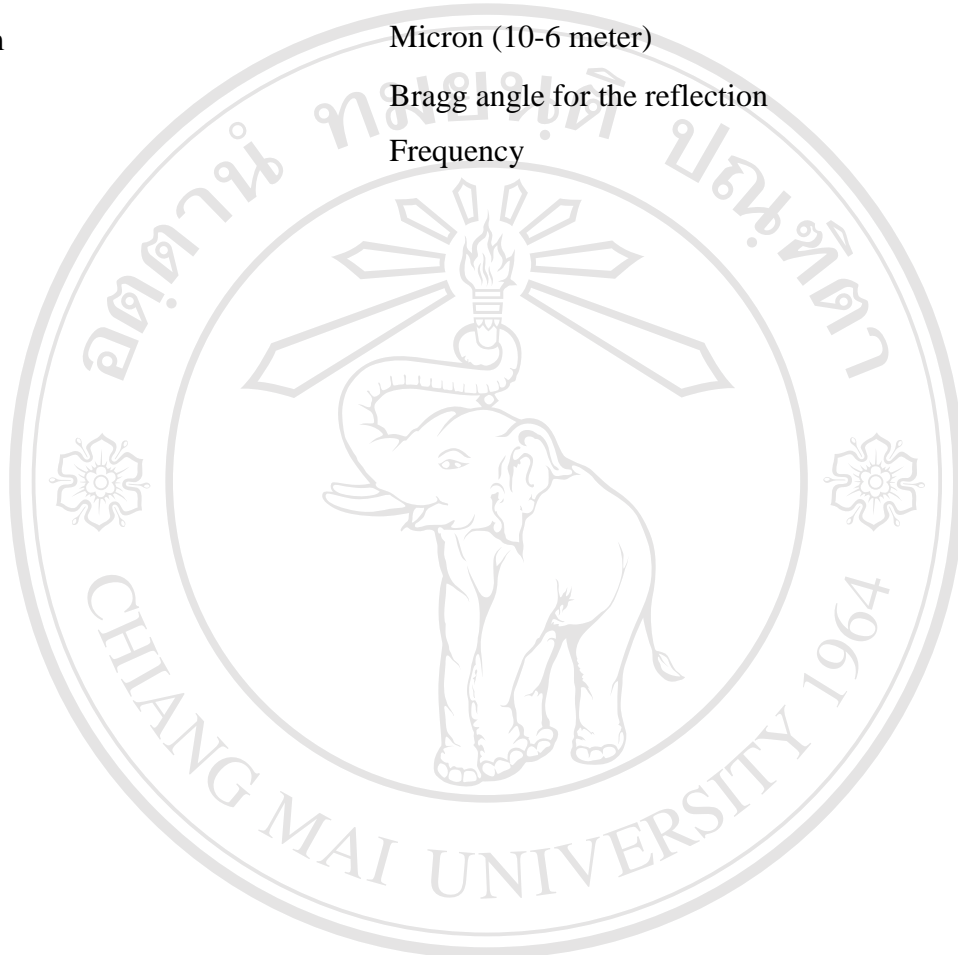
- 3.15 Response of unloaded TiO₂, (a) Pt, (b) Au and (c) Ag-loaded TiO₂ sensors operated at 300–400 °C towards 0.10 vol% CH₃CH₂OH 83
- 3.16 Response (left axis) and response time (T_{res}) (right axis) of unloaded TiO₂, 0.75 mol% metal-loaded TiO₂ sensors to different concentration of CH₃CH₂OH at 350 °C 84
- 3.17 The change in resistance of 0.75 mol% Pt, Au and Ag-loaded TiO₂ sensors, under exposure to (CH₃)₂CO pulses with varying concentrations from 0.0050 to 0.10 vol% 350 °C 86
- 3.18 Response of unloaded TiO₂, (a) Pt, (b) Au and (c) Ag-loaded TiO₂ sensors operated at 300–400 °C towards 0.2 vol% (CH₃)₂CO 87
- 3.19 Response (left axis) and response time (T_{res}) (right axis) of unloaded TiO₂ and metal-loaded TiO₂ sensors to different concentration of (CH₃)₂CO at 400 °C 88
- 3.20 The change in resistance of 0.50 mol% Pt, Au and Ag-loaded TiO₂ sensors, under exposure to carbon monoxide pulses with varying concentrations from 0.0050 to 0.10 vol% 350 °C 89
- 3.21 Response of unloaded TiO₂, (a) Pt and (b) Au-loaded TiO₂ sensors operated at 300–400 °C towards 0.10 vol% carbon monoxide 90
- 3.22 The change in resistance of 0.50 mol% Pt, Au and Ag-loaded TiO₂ sensors, under exposure to SO₂ pulses with varying concentrations from 0.0010 to 0.050 vol% 350 °C. 92
- 3.23 The selectivity histograms of (a) Pt, (b) Au and (c) Ag-loaded TiO₂ sensors for explosive gases at concentration of 0.10 vol% and operating temperature of 350 °C 94

A.1	Flame Spray Pyrolysis Reactor at The NRL Research Laboratory Chiang Mai University	141
A.2	X-ray Diffractometer, Rigaku, Miniflex II, Japan	142
A.3	Scanning Electron	
A.4	Microscope & Energy Dispersive X-Ray Spectrometer, JSM-6335F, JEOL, Japan	143
A.5	Transmission Electron Microscope, JEM-2010, JOEL, Japan	144
A.6	Surface area analyzer, Quantachrome Autosorb 1 MP, USA	145
B.1	JCPDS File No. 21-1272 of Titanium Dioxide (Anatase)	146
B.2	JCPDS File No. 21-1276 of Titanium Dioxide (Rutile)	147
B.3	JCPDS File No. 87-0640 of Pt	148
B.4	JCPDS File No. 04-0784 of Au	149
B.5	JCPDS File No. 87-0717 of Ag	150

ABBREVIATIONS AND SYMBOLS

Å	Angstrom
BET	Brunauer-Emmett-Teller
°C	Degree Celsius
CVD	Chemical vapor deposition
d_{BET}	Average BET-equivalent particle diameter
d_{hkl}	Interplanar distance between (hkl) planes
eV	Electron Volt
EDS,EDXS	Energy Dispersive X-ray Spectroscopy
FSP	Flame Spray Pyrolysis
h	Plank's constant (6.63×10^{-34} Js)
h ν	Photon energy
HRTEM	High Resolution Transmission Electron Microscopy
ICDD	International Center for Diffraction Data
JCPDS	Joint Committee Powder Diffraction Standards
K	Kelvin
mg	Milligram
mL	Milliliter
nm	Nanometer (10^{-9} m)
PDF	Powder Diffraction File
pgm	Platinum group metal
PVD	Physical vapor deposition
SAED	Selected Area Electron Diffraction
SEM	Scanning Electron Microscopy
SSA	Specific Surface Area
SSA_{BET}	Specific surface area from BET method
TEM	Transmission Electron Microscopy

TLV	Threshold limit value
XRD	X-ray diffraction
λ	Wavelength
μg	Microgram (10 ⁻⁶ g)
μm	Micron (10 ⁻⁶ meter)
θ	Bragg angle for the reflection
ν	Frequency



ลิขสิทธิ์มหาวิทยาลัยเชียงใหม่
Copyright© by Chiang Mai University
All rights reserved